

Adsorption of L-aspartate to rutile (α -TiO₂): Experimental and theoretical surface complexation studies

Caroline M. Jonsson^{a,b,*}, Christopher L. Jonsson^{a,b}, Charlene Estrada^{a,b},
Dimitri A. Sverjensky^{a,b}, H. James Cleaves II^b, Robert M. Hazen^b

^a Department of Earth & Planetary Sciences, Johns Hopkins University, Baltimore, MD 21218, USA

^b Geophysical Laboratory, Carnegie Institution of Washington, 5251 Broad Branch Road NW, Washington, DC 20015, USA

Received 7 July 2009; accepted in revised form 18 December 2009; available online 11 January 2010

Abstract

Interactions between aqueous amino acids and mineral surfaces influence many geochemical processes from biomineralization to the origin of life. However, the specific reactions involved and the attachment mechanisms are mostly unknown. We have studied the adsorption of L-aspartate on the surface of rutile (α -TiO₂, $\text{pH}_{\text{PPZC}} = 5.4$) in NaCl(aq) over a wide range of pH, ligand-to-solid ratio and ionic strength, using potentiometric titrations and batch adsorption experiments. The adsorption is favored below pH 6 with a maximum of 1.2 μmol of adsorbed aspartate per m^2 of rutile at pH 4 in our experiments. The adsorption decreases at higher pH because the negatively charged aspartate molecule is repelled by the negatively charged rutile surface above pH_{PPZC} . At pH values of 3–5, aspartate adsorption increases with decreasing ionic strength. The adsorption of aspartate on rutile is very similar to that previously published for glutamate (Jonsson et al., 2009). An extended triple-layer model was used to provide a quantitative thermodynamic characterization of the aspartate adsorption data. Two reaction stoichiometries identical in reaction stoichiometry to those for glutamate were needed. At low surface coverages, aspartate, like glutamate, may form a bridging-bidentate surface species binding through both carboxyl groups, i.e. “lying down” on the rutile surface. At high surface coverages, the reaction stoichiometry for aspartate was interpreted differently compared to glutamate: it likely involves an outer-sphere or hydrogen bonded aspartate surface species, as opposed to a partly inner-sphere complex for glutamate. Both the proposed aspartate species are qualitatively consistent with previously published ATR–FTIR spectroscopic results for aspartate on amorphous titanium dioxide. The surface complexation model for aspartate was tested against experimental data for the potentiometric titration of aspartate in the presence of rutile. In addition, the model correctly predicted a decrease of the isoelectric point with increased aspartate concentration consistent with previously published studies of the aspartate–anatase system. Prediction of the surface speciation of aspartate on rutile indicates that the relative proportions of the two complexes are a strong function of environmental conditions, which should be taken into account in considerations of geochemical systems involving the interactions of biomolecules and minerals in electrolyte solutions.

© 2010 Elsevier Ltd. All rights reserved.

1. INTRODUCTION

The interaction of amino acids with mineral surfaces in electrolyte solutions is of great interest to a wide range of

geochemical topics and processes. For example, in theories of the origins of life, amino acid–mineral surface interactions have long been suggested to have played a critical role (Goldschmidt, 1952; Hazen, 2006; Lambert, 2008). Polymerization of amino acids into peptides and chiral selectivity of biomolecules may have been facilitated in the prebiotic era by attachment to mineral surfaces through adsorption processes. However, several different adsorption modes have been suggested for amino acids on mineral sur-

* Corresponding author. Present address: Department of Chemistry, University of Gothenburg, SE-412 96 Gothenburg, Sweden. Tel.: +46 31 786 9066; fax: +46 31 772 1394.

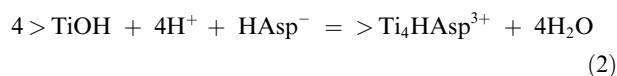
E-mail address: caroline.jonsson@chem.gu.se (C.M. Jonsson).

faces and there is not yet a detailed understanding of exactly how the adsorption takes place at a molecular level (Lambert et al., 2009). Detailed molecular and adsorption studies of glycine on silica have revealed different adsorption mechanisms under different environmental conditions (Costa et al., 2008), but knowledge of the role of amino acid side chains in adsorption on minerals is incomplete. Similarly, in studies of biomineralization processes, there has been a considerable interest in the role of amino acid–mineral surface interactions in the precipitation and growth of mineral skeletal materials. For example, peptides containing the acidic amino acid anions aspartate and glutamate appear to be critically involved in the kinetics of carbonate and phosphate mineral growth and trace element incorporation (Teng and Dove, 1997; Tsortos and Nancollas, 1999, 2002; Elhadj et al., 2006a,b; De Yoreo et al., 2007; Stephenson et al., 2008). However, little is understood about how even monomeric amino acids attach to mineral surfaces, the surface speciation that must exist, and the dependence of the surface speciation on environmental conditions.

Although few studies exist of aspartate adsorption on well-characterized mineral surfaces over a wide range of defined conditions, a variety of very different adsorption mechanisms have been proposed. Adsorption, proton consumption, and electrokinetic measurements and a two-site Stern surface complexation model of aspartate on titanium dioxide (Giacomelli et al., 1995) were interpreted to indicate the reaction



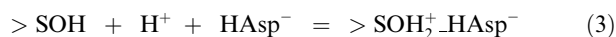
where HAsp^- represents the monovalent aspartate anion. However, the adsorption data as a function of pH refer to only a single ligand-to-solid ratio and two ionic strengths, and contain significant scatter, which contributes to ambiguities in the application of surface complexation models attempting to establish reaction stoichiometries. XPS measurements on dried samples in this system were interpreted as indicating deprotonation of the $-\text{NH}_3^+$ group and inner-sphere attachment of the amine to surface Ti (e.g. $>\text{Ti}-\text{NH}_2-\text{CH}-$) with “weak (if any) interactions” between the unprotonated carboxyl functional groups and the surface (Giacomelli et al., 1995). In contrast, an *in situ* ATR–FTIR study of aspartate on amorphous titanium dioxide (Roddick-Lanzilotta and McQuillan, 2000) depicted a single surface complex of HAsp^- attached to the surface through both carboxyl groups in a bridging-bidentate configuration with the protonated amine group ($-\text{NH}_3^+$) pointing away from the surface. This was inferred to be the only surface complex present over a wide range of pH values and surface loadings but the ionic strength dependence was not considered. Although surface complexation model reactions were not written for this complex, it could be represented in the context of a single-site model by the reaction



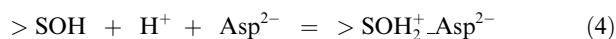
according to which all four oxygens of both carboxyl groups are involved in inner-sphere $>\text{Ti}-\text{O}-\text{C}$ attachments.

The fundamental difference with Eq. (1) is the number of surface sites involved, i.e. four in Eq. (2) based on the ATR–FTIR spectroscopic study (Roddick-Lanzilotta and McQuillan, 2000) and one in Eq. (1) based on the adsorption and surface complexation study (Giacomelli et al., 1995). However both studies inferred inner-sphere surface complexation only.

In contrast to the studies discussed above for aspartate–titanium dioxide systems, aspartate interaction with kaolinite has been suggested to involve only outer-sphere or hydrogen bonded attachments, based on potentiometric titration, adsorption and surface complexation studies (Ikhsan et al., 2004a,b). In the context of an extended constant capacitance model with generic variable charge surface sites ($>\text{SOH}$) the adsorption was represented by the reactions

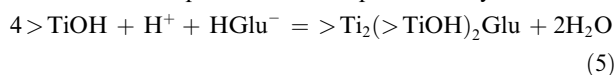


and

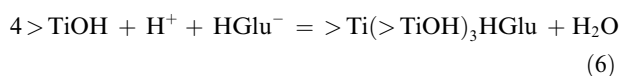


The surface complexes in Eqs. (3) and (4) were inferred to represent outer-sphere protonated and deprotonated aspartate, respectively. However, only a single ionic strength was used and a limited range of aspartate concentrations were tested. Under these circumstances, it is again the case that considerable ambiguities exist in the deduction of reaction stoichiometries through the application of surface complexation modeling.

The behavior of aspartate at the mineral–water interface might be expected to be similar to that of glutamate because of the similarities in molecular structure and of the aqueous protonation reactions. Indeed, the bridging-bidentate complex of aspartate on amorphous titanium dioxide discussed above was suggested to be the same as an analogous bridging-bidentate complex for glutamate on amorphous titanium dioxide (Roddick-Lanzilotta and McQuillan, 2000). In contrast to the single aspartate complex inferred in the ATR–FTIR study, the bridging-bidentate complex of glutamate was one of several complexes inferred for glutamate in the same study. However, our theoretical modeling indicates that the specific bridging-bidentate reaction stoichiometry in Eq. (2), involving four inner-sphere $>\text{Ti}-\text{O}-\text{C}$ attachments is highly unlikely. Our surface complexation modeling of the formation of a glutamate bridging-bidentate complex on amorphous ferric hydroxide and rutile (Sverjensky et al., 2008; Jonsson et al., 2009) suggested that the reactions do not involve four inner-sphere $>\text{M}-\text{O}-\text{C}$ attachments. Instead, a bridging-bidentate complex with only one or two inner-sphere $>\text{M}-\text{O}-\text{C}$ attachments is indicated. Such complexes can be represented by



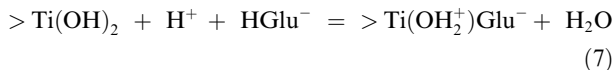
or



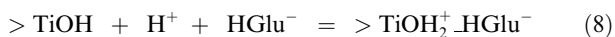
i.e. partly inner-sphere and partly outer-sphere attachments of the carboxyl oxygens to the surface Ti. Eqs. (5) and (6)

cannot be distinguished by surface complexation modeling alone because the reaction stoichiometries are so similar and the electrostatic work contributions are identical.

Eq. (5) refers to two inner-sphere $>\text{Ti}-\text{O}-\text{C}$ attachments and two hydrogen bonded attachments of oxygens from the carboxyl groups, and the glutamate is deprotonated (containing an $-\text{NH}_2$ group) consistent with the state of protonation for aspartate inferred by [Giacomelli et al. \(1995\)](#). Eq. (6) refers to one inner-sphere $>\text{Ti}-\text{O}-\text{C}$ attachment and three hydrogen bonded attachments of oxygens from the carboxyl groups, and the glutamate is protonated (contains an $-\text{NH}_3^+$ group) consistent with the work of [Roddick-Lanzilotta and McQuillan \(2000\)](#). In addition, our surface complexation studies indicate that the bridging-bidentate glutamate complex predominates on the rutile and ferric hydroxide surfaces at low pH values and low surface coverages. At high surface coverages, we inferred that glutamate forms a second surface complex that “stands up” on the surface consistent with the reaction stoichiometry



or



(cf. Eq. (4)). The surface complex in Eq. (7) can be interpreted as representing a deprotonated glutamate attached to the surface by one inner-sphere linkage and one hydrogen bonded linkage. Eq. (8) represents the formation of a hydrogen bonded or outer-sphere complex. Eqs. (5) and (7) are consistent with the spectroscopic observations and inferences of [Roddick-Lanzilotta and McQuillan \(2000\)](#). Whether or not the putative bridging-bidentate complex of aspartate on titanium dioxide involves the same reaction stoichiometry as for glutamate, and whether additional surface complexes of aspartate form remain to be established.

The present work is part of a larger study aimed at gaining a fundamental understanding of the speciation of amino acids at the mineral–water interface under widely varying environmental conditions. This paper is focused on experimental potentiometric titrations of the aspartate–rutile–electrolyte–water system and adsorption measurements of aspartate on rutile over a wide range of pH values, ionic strengths and ligand-to-solid ratios. The experimental results are integrated with a surface complexation model, which establishes the stoichiometry of the adsorption reactions and provides a thermodynamic characterization of the equilibria involved. In a parallel study, we will be reporting ATR–FTIR spectroscopic measurements of both aspartate and glutamate on rutile together with theoretical molecular calculations on these systems. We focused on rutile in the present study because it is a model colloidal substance: identically prepared rutile samples have been the subject of numerous intensive studies of proton and cation adsorption ([Machesky et al., 1998](#); [Ridley et al., 1999, 2004, 2005](#); [Fedkin et al., 2003](#); [Zhang et al., 2004](#)). Rutile was also probably present on the prebiotic Earth ([Hazen et al., 2008](#)), which makes it relevant to origin of life studies. Finally, experimental results for the relatively simple aspartate–rutile–electrolyte–water system enable a quantitative

thermodynamic characterization of aspartate adsorption, which can then be extrapolated to compositionally more complex systems in two ways. First, the equilibrium constants for aspartate adsorption can be included in extended triple-layer models involving additional sorbates such as Ca^{2+} , Mg^{2+} , SO_4^{2-} and glutamate characterized previously ([Sverjensky, 2005, 2006](#); [Sverjensky and Fukushi, 2006b](#); [Jonsson et al., 2009](#)). Second, models for all these adsorbates on rutile can be readily extrapolated to other more geochemically abundant minerals with the aid of the Born solvation theory ([Sverjensky and Fukushi, 2006a](#); [Fukushi and Sverjensky, 2007](#)). As a consequence, it becomes possible to make quantitative predictions that can facilitate evaluation of the potential role of mineral surface chemistry in the origin of life and other geochemical realms of interest.

2. MATERIALS AND METHODS

2.1. Materials

All solutions and suspensions were made from milliQ-water (Millipore, resistance = $18.2 \text{ M}\Omega \text{ cm}^{-1}$) with NaCl (Fisher BioReagents p.a., dried at 180°C) used to provide a constant ionic medium of 0.01, 0.1 and 0.3 M NaCl, respectively. The parenthesis around Cl indicates that the chloride ion concentration was allowed to vary, while the sodium ion concentration was held constant throughout the experiments. Stock solutions of HCl (J.T. Baker, p.a.) were standardized against tris(hydroxymethyl)aminomethane (Trizma base, Fisher Scientific 99.9%), and NaOH (J.T. Baker) solutions were standardized against these standardized HCl solutions. L-Aspartic acid (Acros Organics 98+%) was used without further purification, since there was no sign of contamination of the L-aspartic acid powder. Also, the potentiometric titrations performed on the dissolved amino acid were stable and reproducible, and consistent with published pK_a values (see below). For amino acid analysis, the following chemicals were used without further purification: ninhydrin (Aldrich, 97%), 2-methoxyethanol (Sigma–Aldrich, 99.9%), acetic acid (Sigma–Aldrich, 99%), sodium acetate (Sigma–Aldrich, 99%), NaCN (Fisher) and ethanol (The Warner Graham Company, 200 proof).

The rutile sample used in the present study was from the same extensively cleaned and well-characterized batch previously described by [Jonsson et al. \(2009\)](#), courtesy of J. Rosenqvist, D. Wesolowski and M. Machesky. Scanning electron microscopy (SEM) showed that the rutile crystals are needle-shaped and approximately 50–100 nm wide and 400–500 nm long. The most clearly visible faces are (1 1 0) parallel to the length of the crystals and (1 0 1) and (1 1 1) as terminating faces. The specific surface area was determined to $18.1 \text{ m}^2 \text{ g}^{-1}$ using the BET N_2 adsorption method ([Brunauer et al., 1938](#)).

For this particular rutile sample, a pH_{PPZC} around pH 5.4 is well established in the literature ([Machesky et al., 1998](#); [Ridley et al., 2002](#); [Fedkin et al., 2003](#)) and was also confirmed during our previous potentiometric titration study ([Jonsson et al., 2009](#)). In the latter study, we established the point of zero salt effect (pH_{PZSE}) of rutile in NaCl

solutions as 5.37 (± 0.1), which was used to estimate the pristine point of zero charge, $\text{pH}_{\text{PPZC}} = 5.4$ (± 0.1) with the relation

$$\text{pH}_{\text{PPZC}} = \text{pH}_{\text{PZSE}} + 0.5(\log K_{\text{Cl}^-}^{\theta} - \log K_{\text{Na}^+}^{\theta}) \quad (9)$$

using theoretically calculated values of $\log K_{\text{Na}^+}^{\theta}$ and $\log K_{\text{Cl}^-}^{\theta}$ (Sverjensky, 2005). This method has been established consistent with the point of zero salt effects and isoelectric points of a wide range of oxides and electrolytes. Our result for $\text{pH}_{\text{PPZC}} = 5.4$ is also identical to the value obtained by (Machesky et al., 1998) with several ionic strengths.

2.2. Experimental methods

2.2.1. Potentiometric titrations

Automated potentiometric titrations of the systems aspartate–NaCl and aspartate–rutile–NaCl were carried out with a titrator (Metrohm 836 Titrand) equipped with two dosimeters (800 Dosino), a propeller stirrer, and a combination electrode (Metrohm Ecotrode Plus) that was calibrated with standardized pH buffers (Fisher Scientific). The temperature was kept constant at 25 ± 0.1 °C by a thermostatic water bath (Lauda RE104) allowing water to circulate outside the titration vessel. CO₂ was kept out of the system by a continuous flow of zero grade argon gas that was further purified using several gas washing bottles containing: (1) nothing, (2) H₂SO₄ 10%, (3) NaOH 2%, and (4) NaCl 0.1 M, respectively. Stable potentials within ± 0.1 mV were usually reached within 10–30 min after each addition of acid or base. Precautions were taken to ensure that there were no photocatalytic or microbiological effects that could significantly affect the data (Jonsson et al., 2009). Titration data for the aspartate–NaCl system are presented in plots showing the net acid added per mole of aspartate (m_{H}) according to

$$m_{\text{H}} = \frac{([\text{H}]_{\text{added}} - \{\text{H}^+\}_{\text{aq}}) - ([\text{OH}]_{\text{added}} - \{\text{OH}^-\}_{\text{aq}})}{[\text{Asp}]_{\text{tot}}} \quad (10)$$

For the aspartate–rutile–NaCl system the data are presented as the moles of net acid added per m² of rutile (N_{H}) according to

$$N_{\text{H}} = \frac{([\text{H}]_{\text{added}} - \{\text{H}^+\}_{\text{aq}}) - ([\text{OH}]_{\text{added}} - \{\text{OH}^-\}_{\text{aq}})}{A_s C_s} \quad (11)$$

where A_s and C_s represent the BET surface area (m² g⁻¹) and solid concentration of particles (g L⁻¹), respectively.

In Eqs. (10) and (11), $[\text{H}]_{\text{added}}$ and $[\text{OH}]_{\text{added}}$ are defined by the concentration of added acid or base, respectively, in the total volume after each addition of acid or base during the titration, while $\{\text{H}^+\}_{\text{aq}}$ and $\{\text{OH}^-\}_{\text{aq}}$ were determined during the pH measurements.

2.2.2. Batch adsorption experiments

Quantitative adsorption of aspartate on rutile was studied at 25 ± 1 °C and 1 bar. Batch samples with a solid concentration of 20 g L⁻¹ and a total concentration of L-aspartate ranging from 0.1 to 1 mM (0.3 to 2.7 $\mu\text{mol m}^{-2}$) were prepared in 15 mL Falcon tubes. In order to cover the pH range 3–10, precise volumes of standardized HCl

or NaOH were added to each sample. Argon gas, purified as described above, was purged through the suspensions to avoid contamination by CO₂ from air. Preliminary experiments indicated that the adsorption of aspartate reached a steady state within the first 3 h after addition of aspartate to a rutile suspension. In the present work, batch samples were equilibrated on a test tube rotator (Labroller II, Labnet International, Inc., H5100) for 16–20 h. After this, pH ($-\text{Log}\{\text{H}^+\}$) was measured with a combination glass electrode (Thermo-Electron, Orion 8103BNUWP), that was previously calibrated with standardized pH buffers (Fisher Scientific). In order to separate the aqueous solution from the solid phase, the samples were centrifuged for 10 min at a relative centrifugal force of 1073g (Fisher Scientific accuSpin 400). The concentration of aspartate in the supernatant was measured with UV–vis spectroscopy (Hewlett–Packard, 8452A, Diode Array spectrophotometer) using the ninhydrin-labeling technique, as described previously by Jonsson et al. (2009) and references therein. By calculating the difference between the known total concentration and the concentration remaining in the supernatant after equilibration, the quantity of aspartate adsorbed on the surface of rutile was determined in each sample.

2.3. Surface complexation approach

We applied the extended triple-layer model (ETLM) of surface complexation (Sverjensky, 2005, 2006; Sverjensky and Fukushi, 2006b) to our titration and adsorption data. This approach specifically accounts for the electrical work associated with desorption of chemisorbed water molecules during inner-sphere surface complexation. As a consequence, it indicates the number of inner-sphere linkages (e.g. >Ti–O–C) for the adsorbate, as well as the number of Ti surface sites involved in the reaction stoichiometry. These results can significantly constrain the likely mode of surface attachment. The calculations reported below were carried out iteratively with the computer code GEOSURF described previously (Sahai and Sverjensky, 1998). We used the same surface protonation and electrolyte adsorption parameters established in our previous study (Jonsson et al., 2009) of the rutile–NaCl system (Table 1). With this basis, we formulated adsorption reactions for aspartate on rutile using the species suggested in the ATR–FTIR study of aspartate on amorphous titanium dioxide and the surface complexation models of aspartate and glutamate on rutile and amorphous titanium dioxide discussed above (Eqs. (2)–(8)). Iterative application of the surface complexation calculations to our experimental adsorption data over a wide range of pH values, ionic strengths and ligand-to-solid ratios enabled testing the above reaction stoichiometries, as well as many others, to find the most appropriate reaction stoichiometries for aspartate on rutile. The calculation results were then tested for consistency with potentiometric titration results for the aspartate–rutile–NaCl system. Theoretical prediction of the migration of the isoelectric point with increasing aspartate concentration compared with experimental data from Giacomelli

Table 1

Aqueous aspartate properties^a, rutile (α -TiO₂) characteristics^b and extended triple-layer model parameters for proton, electrolyte, and aspartate adsorption on rutile.

Reaction type	Reaction	Log <i>K</i>
Aqueous aspartate equilibria	Asp ²⁻ + H ⁺ = HAsp ⁻	10.01
	HAsp ⁻ + H ⁺ = H ₂ Asp	3.88
	H ₂ Asp + H ⁺ = H ₃ Asp ⁺	1.92
	HAsp ⁻ + Cl ⁻ + 2H ⁺ = H ₃ AspCl	5.3
	HAsp ⁻ + Na ⁺ = NaHAsp	-0.3
	HAsp ⁻ + Na ⁺ = NaAsp ⁻ + H ⁺	-9.6
Surface equilibria	Hypothetical 1.0 m standard state	
log <i>K</i> ₁ ⁰	> TiOH + H ⁺ = > TiOH ₂ ⁺	2.52
log <i>K</i> ₂ ⁰	> TiO ⁻ + H ⁺ = > TiOH	8.28
log * <i>K</i> _{Na⁺} ⁰	> TiOH + Na ⁺ = > TiO ⁻ .Na ⁺ + H ⁺	-5.6
log * <i>K</i> _{Cl⁻} ⁰	> TiOH + H ⁺ + Cl ⁻ = > TiOH ₂ ⁺ .Cl ⁻	5.0
log * <i>K</i> _{>Ti₂(>TiOH)₂Asp} ⁰	4 > TiOH + H ⁺ + HAsp ⁻ = > Ti ₂ (> TiOH) ₂ Asp + 2H ₂ O	16.5(±0.2)
log * <i>K</i> _{>TiOH₂⁺.HAsp⁻} ⁰	> TiOH + H ⁺ + HAsp ⁻ = > TiOH ₂ ⁺ .HAsp ⁻	7.9(±0.2)
Surface equilibria	Site-occupancy standard states ^c	
log <i>K</i> _{>Ti₂(>TiOH)₂Asp} ⁰	2 > TiOH ₂ ⁺ + 2 > TiOH + HAsp ⁻ = > Ti ₂ (> TiOH) ₂ Asp + H ⁺ + 2H ₂ O	20.8(±0.3)
log <i>K</i> _{>TiOH₂⁺.HAsp⁻} ⁰	> TiOH ₂ ⁺ + HAsp ⁻ = > TiOH ₂ ⁺ .HAsp ⁻	5.4(±0.3)

^a Protonation constants and electrolyte ion pair constants from De Robertis et al. (1991).

^b Rutile properties are $N_s = 3.0$ sites nm⁻², $A_s = 18.1$ m² g⁻¹, $C_1 = 120$ μF cm⁻², $C_2 = 120$ μF cm⁻², pH_{PPZC} = 5.4, $\Delta pK_n^0 = 6.3$, log *K*₁⁰ = 2.25, log *K*₂⁰ = 8.50, log *K*_{Na⁺}⁰ = 2.68, log *K*_{Cl⁻}⁰ = 2.48 (Jonsson et al., 2009).

^c Equilibrium constants relative to site-occupancy standard states were also written relative to charged surface sites calculated using the equations: log *K*_{>Ti₂(>TiOH)₂Asp}⁰ = log **K*_{>Ti₂(>TiOH)₂Asp}⁰ + log $\frac{(N_s A_s)^2 C_s^3}{100} - 2\text{pH}_{\text{PPZC}} + \Delta pK_n^0$; log *K*_{>TiOH₂⁺.HAsp⁻}⁰ = log **K*_{>TiOH₂⁺.HAsp⁻}⁰ + log $\frac{(N_s A_s)}{100} - \text{pH}_{\text{PPZC}} + \frac{\Delta pK_n^0}{2}$, where N_s is site density (sites nm⁻²), A_s is BET surface area (m² g⁻¹), and C_s is solid concentration (g L⁻¹).

et al. (1995) also served as a qualitative test of the surface complexation model developed below.

3. RESULTS AND DISCUSSION

3.1. Titration of aqueous aspartate

The symbols in Fig. 1a represent data from two potentiometric titrations of aqueous aspartate in 0.01 and 0.1 M NaCl, respectively, over the pH range from 3 to 10. This range covers the protonation of the amine and the γ -carboxyl groups (Table 1). The overall reproducibility of the experimental data is within ± 0.02 mol of protons per mole of aspartate. The solid lines in Fig. 1a represent theoretical predictions of the titrations using equilibrium constants in Table 1. The equilibrium constants for aqueous protonation of aspartate and electrolyte ion-pairing with aspartate were taken from the literature (De Robertis et al., 1991). Aqueous activity coefficients were calculated using the extended Debye–Huckel equation (Helgeson et al., 1981) using electrolyte characteristics described previously (Criscenti and Sverjensky, 2002). Uncertainties in the aspartate protonation and electrolyte ion-pairing constants probably contribute the largest uncertainty to the calculated curve, of the order of ± 0.05 mol of protons per mole of aspartate. It can be seen in Fig. 1a that the calculated lines agree with the experimental data within the estimated uncertainties.

The calculated aqueous speciation of aspartate in 0.1 M NaCl is shown in Fig. 1b. As expected, the predominant species are aspartate with different protonation levels but the electrolyte ion-pairs do contribute to some extent. At

lower NaCl concentrations, the contribution from the ion-pairs is smaller.

3.2. Adsorption of aspartate on rutile

Adsorption data for L-aspartate on rutile in 0.1 M NaCl are shown in Fig. 2a and c. The total concentration of aspartate ranged from 0.1 to 1 mM (0.3 to 2.7 μmol m⁻²) and the solid concentration was 20 g L⁻¹. In all cases, the largest amount of aspartate was adsorbed at a pH value of about 4. It is expected that aspartate will adsorb at this pH because 50% of the aqueous aspartate has a negative charge under these conditions (Fig. 1b) and the rutile surface is mostly positively charged below a pH of about 5.4. The adsorption decreases at higher pH because the negatively charged aspartate molecule is repelled by the negatively charged rutile surface. Adsorption also decreases below a pH of 4 because aspartate exists predominantly in a net neutral form in aqueous solution under these conditions. It can also be seen in Fig. 2a that the highest amount of adsorbed aspartate is about 1.2 μmol m⁻². The estimated experimental uncertainty in Fig. 2 might be a maximum of ± 0.05 μmol m⁻², based on the reproducibility between duplicate batch runs, as well as the stability in the UV–vis spectroscopic measurements.

Batch adsorption experiments performed at different background electrolyte concentrations are shown in Fig. 2b and d. The NaCl concentrations used were 0.01, 0.1 and 0.3 M, respectively, while the total concentration of aspartate was kept constant at 0.5 mM (1.4 μmol m⁻²) in all experiments.

Data for $3 < \text{pH} < 5$, which is the interval where aspartate adsorbs to the highest extent, indicate a possible small increase in adsorption with decreasing ionic strength. On average, the difference in aspartate adsorption between highest and lowest electrolyte concentrations at $3 < \text{pH} < 5$ is $0.15 \mu\text{mol m}^{-2}$, which corresponds to a 20% difference in the total amount of adsorbed aspartate. Between pH values of 5.5 and 6.5 there is no significant dispersion of the data. Some ionic strength dependence might exist above a pH of about 6.5, although opposite trends are observed compared to low pH values. Due to the low amount of adsorbed aspartate at these high pH values, the relative uncertainty of the results are higher and it is dif-

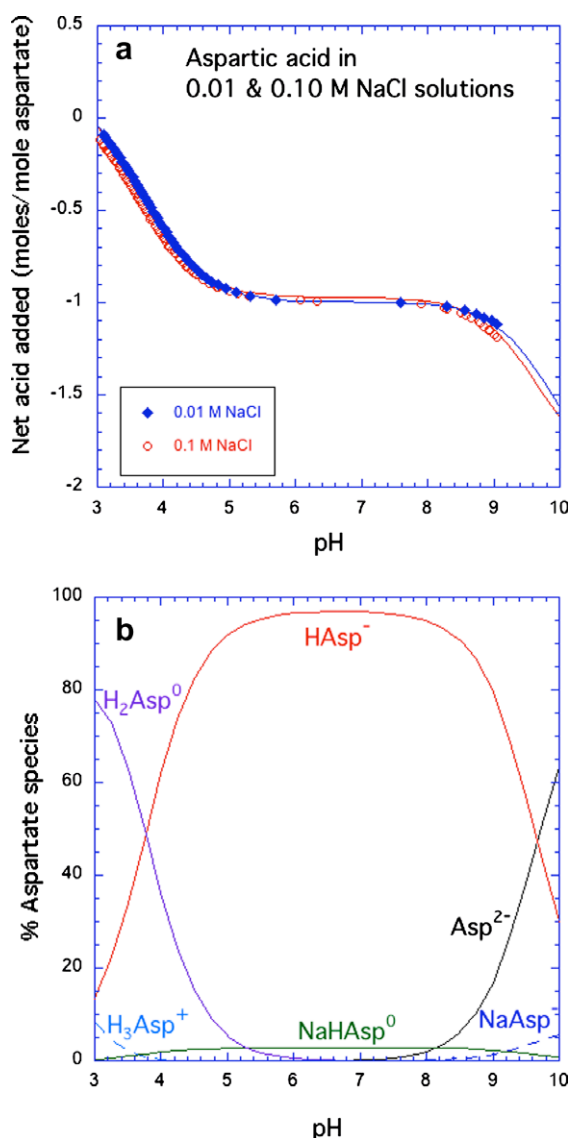
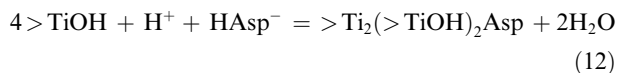


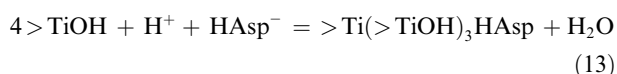
Fig. 1. (a) Potentiometric titration data for aqueous aspartate in 0.01 and 0.1 M NaCl, respectively; (b) calculated aqueous speciation of aspartate in 0.1 M NaCl. Symbols represent experimental data. The solid curves were calculated using the aqueous aspartate protonation and electrolyte ion-pairing equilibrium constants in Table 1.

ficult to draw reliable conclusions about a possible ionic strength dependence in this region from the data alone.

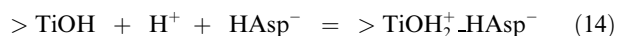
Two basic types of reaction stoichiometry were needed to describe the adsorption data plotted in Fig. 2



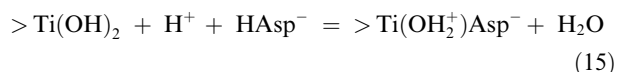
or



and



or



As noted above, the reactions in Eqs. (12) and (13) cannot be distinguished by surface complexation modeling and neither can Eqs. (14) and (15). But one reaction from each pair is needed to describe the adsorption data. Possible ways in which the surface aspartate species in Eqs. (12)–(15) might be interpreted to attach to rutile are indicated in Fig. 3a–d. It should be emphasized that these are highly idealized representations based on fragments of the bulk crystal structure of rutile. It has been assumed in these pictures that inner-sphere bonds between aspartate and the rutile involve terminal oxygens of the type $> \text{TiOH}_2^+$ or $> \text{Ti}(\text{OH}_2^+)_2$, because terminal oxygens have been identified as being involved in ligand exchange reactions for other oxyanions and oxide surfaces (Catalano et al., 2006, 2007). Outer-sphere or hydrogen bonding interactions may involve a number of functional groups at the rutile surface including the bridging $> \text{Ti}_2\text{OH}$ groups shown in Fig. 3. The two surface complexes on the right-hand side of Eqs. (12) and (13), referred to here as bridging-bidentate species, are represented in Fig. 3a and b, respectively. Both have four points of attachment of the aspartate to the surface and can be thought of as partly inner-sphere and partly hydrogen bonded, i.e. the aspartate molecule can be thought of as “lying down” on the surface. For the surface complex in Eq. (12), two attachment points are inner-sphere and two are hydrogen bonded (Fig. 3a). For the surface complex in Eq. (13), one attachment point is inner-sphere and three are hydrogen bonded (Fig. 3b). An alternative scenario to Fig. 3b would involve switching the roles of the two carboxyl groups. It is assumed here in Fig. 3a and b that the inner-sphere bonds involve Ti–O–C linkages and the hydrogen bonds possibly involve $\text{TiOH} \cdots \text{O}=\text{C}$ linkages. Fig. 3a is more closely consistent with the inferences made by Roddick-Lanzilotta and McQuillan (2000), who suggested that the environment of both carboxyl groups at the surface was the same.

Even though Eqs. (14) and (15) cannot be distinguished by surface complexation, the two surface aspartate species are very different. It can be seen in Fig. 3c and d that $> \text{TiOH}_2^+ \text{HAsp}^-$ is an outer-sphere or H-bonded species, but $> \text{Ti}(\text{OH}_2^+) \text{Asp}^-$ is inner-sphere (one water

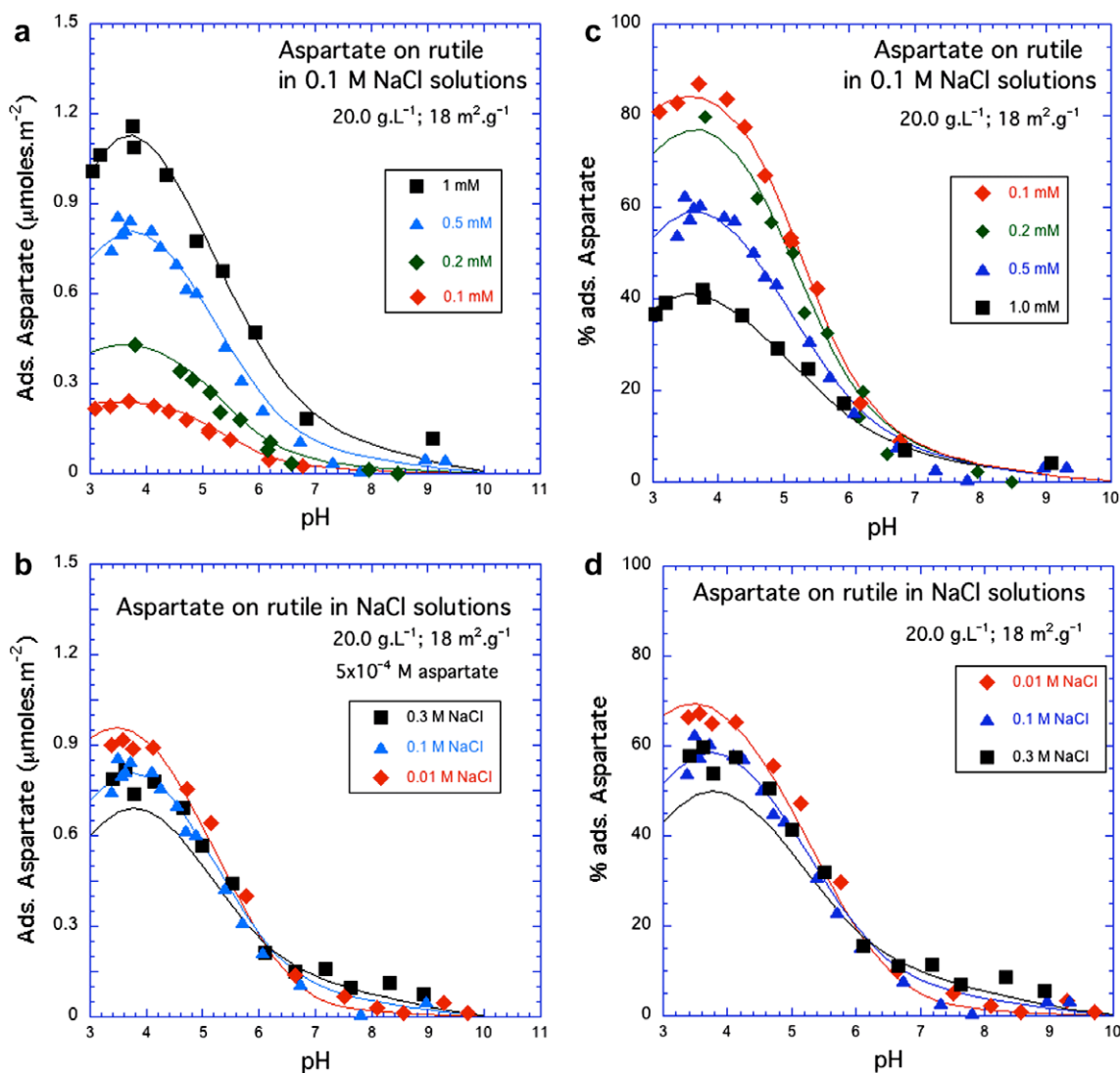


Fig. 2. Adsorption of aspartate on rutile as a function of pH at varying ligand concentrations: (a) ads. in $\mu\text{mol m}^{-2}$, and (c) ads. in %, respectively, and at varying ionic strengths, (b) ads. in $\mu\text{mol m}^{-2}$, and (d) ads. in %, respectively. The symbols represent experimental data. The solid curves were calculated using the surface complexation model with parameters from Table 1. Numerical values of the experimental adsorption data are presented in the [electronic annex](#).

released). Roddick-Lanzilotta and McQuillan (2000) inferred only a single inner-sphere aspartate surface species, which we have attributed to Eq. (12). Consequently, we propose that the additional surface species needed to describe the adsorption data is consistent with Eq. (14) rather than Eq. (15). An outer-sphere species such as in Eq. (14) would not have been readily detectable in the ATR–FTIR study. Overall then, we propose that Eqs. (12) and (14) are the most appropriate reaction stoichiometries for aspartate on rutile. This contrasts with our interpretation for glutamate on rutile, where both surface glutamate species were assumed to be inner-sphere, based on Roddick-Lanzilotta and McQuillan (2000) who inferred at least two inner-sphere species for glutamate on amorphous titanium dioxide.

The reactions in Eqs. (12) and (14) correspond to the equilibrium constants

$$\log^* K_{>\text{Ti}_2(>\text{TiOH})_2\text{Asp}}^0 = \frac{a_{>\text{Ti}_2(>\text{TiOH})_2\text{Asp}} a_{\text{H}_2\text{O}}^2}{a_{>\text{TiOH}}^4 a_{\text{H}^+} a_{\text{HAsp}^-}} 10^{\frac{F\Delta\psi_{r,12}}{2.303RT}} \quad (16)$$

and

$$\log^* K_{>\text{TiOH}_2^+ \text{HAsp}^-}^0 = \frac{a_{>\text{TiOH}_2^+ \text{HAsp}^-}}{a_{>\text{TiOH}} a_{\text{H}^+} a_{\text{HAsp}^-}} 10^{\frac{F\Delta\psi_{r,14}}{2.303RT}} \quad (17)$$

where the superscripts “*” and “0” refer to reactions written relative to $>\text{TiOH}$, and to the hypothetical 1.0 M standard state for both the surface and aqueous species (Sverjensky, 2003). The terms involving $\Delta\psi_{r,12}$ and $\Delta\psi_{r,14}$ in Eqs. (16) and (17) represent the electrical work involved in the reaction. In the ETLM, the electrical work includes contributions not only for the ions going on or off the surface, but also for the water dipoles coming off the surface in Eq. (12), as explained in (Sverjensky and Fukushima, 2006b). The latter contribution to $\Delta\psi_r$ is $-n_{\text{H}_2\text{O}}(\psi_0 - \psi_\beta)$, where

$n_{\text{H}_2\text{O}}$ represents the number of moles of water on the right-hand side of the reaction. In Eq. (12), $n_{\text{H}_2\text{O}} = 2$, which results in $\Delta\psi_{r,12} = 0$, whereas $\Delta\psi_{r,14} = \psi_0 - \psi_\beta$. In Eqs. (13) and (15), $\Delta\psi_{r,13} = 0$ and $\Delta\psi_{r,15} = \psi_0 - \psi_\beta$, the same result as for Eqs. (12) and (14).

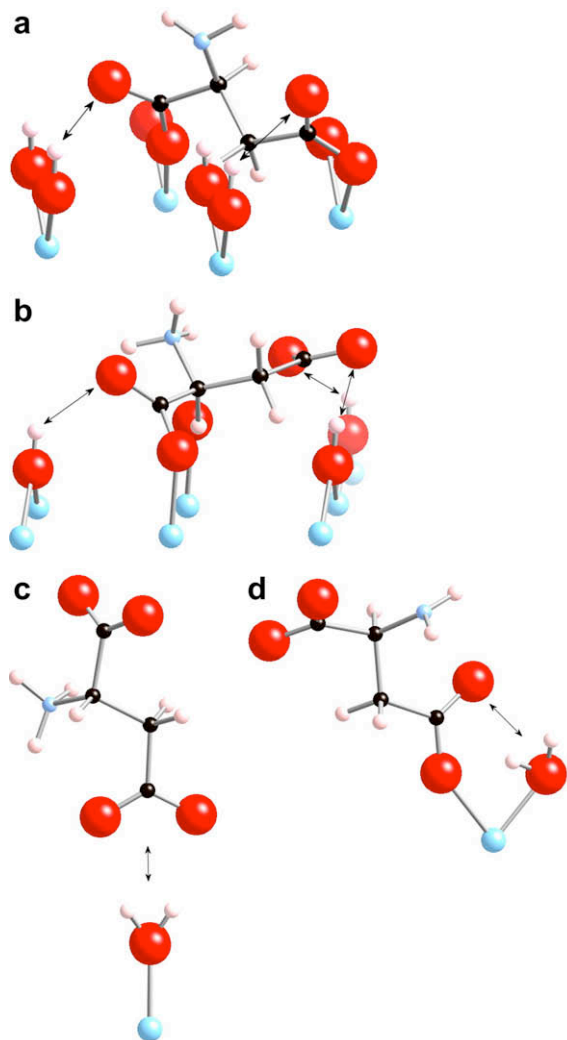


Fig. 3. Possible surface species representing different modes of attachment of aspartate to rutile surface sites, consistent with the surface complexation calculations in the present study. Large spheres indicate oxygen atoms, small filled spheres carbon, small pale spheres hydrogen or nitrogen, and the lowermost spheres titanium at the rutile surface (to scale). Double-headed arrows represent hydrogen bonds. (a) Bridging-bidentate species with four points of attachment involving one inner-sphere Ti–O–C bond and one Ti–OH...O=C hydrogen bond for each carboxyl group (Eq. (12)). (b) Alternative to the bridging-bidentate species in (a). This bridging-bidentate species has four points of attachment involving one inner-sphere Ti–O–C bond and one Ti–OH...O=C hydrogen bond of the α -carboxyl group, and one Ti–OH...O=C hydrogen bond and one Ti–OH...O=C hydrogen bond of the γ -carboxyl group (stabilized through resonance) (Eq. (13)). (c) Outer-sphere or hydrogen bonded aspartate surface species (Eq. (14)). (d) Alternative to the outer-sphere species in (c), chelating species with two points of attachment involving one inner-sphere Ti–O–C bond and one Ti–OH₂⁺...O=C to a single titanium (Eq. (15)).

The solid curves in Fig. 2 represent regression calculations using the reactions in Eqs. (12) and (14). In these calculations, a site density of 3.0 (± 0.5) sites nm⁻² was found to be the most appropriate site density, as in the case of glutamate. This site density is significantly less than what might be expected if adsorption took place on an idealized (1 1 0) surface of rutile. The (1 1 0) plane appears to be the predominant surface exposed on our rutile sample as noted above. On this plane, the abundances of >TiOH₂⁺ and >Ti₂OH sites should both be 5.2 sites nm⁻². However, there are no >Ti(OH₂⁺)₂ sites on this idealized surface. If >Ti(OH₂⁺)₂ sites are involved in the adsorption to a significant extent, the possibility arises that the (1 1 0) surfaces on our sample may contain additional steps of other faces. In any case, the site density obtained by regression is only a fraction of that estimated from crystallographic considerations. Detailed transmission electron microscopic observations of the rutile sample might be able to shed light on this apparent discrepancy. The regression calculations generated values of the equilibrium constants for aspartate adsorption represented by $\log^* K_{>\text{Ti}_2(>\text{TiOH})_2\text{Asp}}^0$ and $\log^* K_{>\text{TiOH}_2^+\text{-HAsp}^-}^0$ in Table 1. Estimated uncertainties are ± 0.2 in the log K values. Based on the estimated experimental uncertainties and the uncertainties in the regression parameters, the calculated curves in the figures show relatively small discrepancies with the experimental data. Clearly, the two reactions are sufficient to describe aspartate adsorption on rutile as a function of pH, ligand-to-solid ratio and ionic strength. The regression values of the equilibrium constants were converted to values of $\log K_{>\text{Ti}_2(>\text{TiOH})_2\text{Asp}}^\theta$ and $\log K_{>\text{TiOH}_2^+\text{-HAsp}^-}^\theta$ referring to site-occupancy standard states and referenced to >TiO⁻ using equations and the values of N_s (site density), A_s (BET surface area), C_s (solid concentration), pH_{PPZC}, and ΔpK_n^θ given in Table 1. The values of log K_j^θ for the j th species in Table 1 are independent of the individual sample characteristics. Consequently, values of log K_j^θ are useful for comparing the binding of aspartate on different oxides. Our equilibrium constants for aspartate adsorption were tested by predicting the proton uptake for the combined aspartate–rutile–electrolyte system and comparing this with experimental titration data. An additional more qualitative test involved prediction of the migration of the isoelectric point with increasing aspartate concentrations.

3.3. Tests of the surface complexation model

3.3.1. Titration of aspartate on rutile

Potentiometric titrations of rutile in 0.1 M NaCl with various concentrations of aspartate present are represented by the symbols in Fig. 4. Data are given as μmol of net acid added per m² of rutile based on Eq. (11). Consequently, each data point represents the sum of protons involved in aqueous aspartate protonation, surface protonation and electrolyte adsorption on rutile, and aspartate adsorption. The estimated uncertainty in the measurements is about $\pm 0.1 \mu\text{mol m}^{-2}$.

Between pH values of about 7 and 9, the data primarily represent protons involved in aqueous aspartate protonation and surface protonation and electrolyte adsorption, since

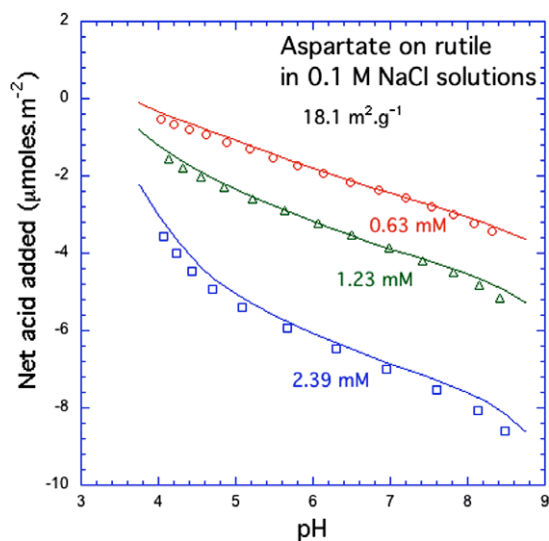


Fig. 4. Potentiometric titrations of rutile in 0.1 M NaCl) in the presence of various concentrations of aspartate. The symbols represent experimental data. The solid curves were calculated using the surface complexation model fitted to the data in Fig. 2.

only a maximum of 0.2 μmol of aspartate is adsorbed per m^2 (8% of the total concentration of aspartate) under these conditions (Fig. 2). Aspartate adsorbs most strongly at about pH 4. Consequently, between pH values of about 4 and 6, the data represent protons involved in aspartate adsorption as well as protons involved in aqueous aspartate protonation, and surface protonation and electrolyte adsorption.

The solid curves in Fig. 4 represent predictions using the surface complexation model developed above and applied in Fig. 2. It can be seen in Fig. 4 that the predicted quantities of net acid added are slightly less negative than observed quantities, especially at higher aspartate concentrations. These discrepancies are close to the estimated uncertainty of about $\pm 0.2 \log K$ units in the surface equilibrium constants for aspartate (Table 1). An additional source of uncertainty in the model arises from uncertainties in the equilibrium constants for the electrolyte adsorption (Jonsson et al., 2009). Nevertheless, the fact that the calculated solid curves have such a similar curvature as the experimental data in the pH range of about 4–6 strongly supports the validity of the proton stoichiometry of the aspartate adsorption reactions in Eqs. (12) and (14).

3.3.2. Migration of the isoelectric point during aspartate adsorption

Electrokinetic studies provide an independent test of the stoichiometry of the reactions in surface complexation models. In particular, electrophoretic mobility studies for a particle suspension at a single ionic strength without an adsorbing ligand present provide a measurement of the isoelectric point (IEP) when the mobility is zero. Adding an adsorbing ligand can result in a displacement of the IEP to either lower or higher pH values depending on the adsorption reaction stoichiometry. In the triple-layer model, the IEP is the pH when the calculated diffuse layer potential at the start of the diffuse layer (ψ_d) is equal to

zero. For the present system, without the adsorbing ligand aspartate, the calculated $\text{IEP} = 5.4$. When aspartate is included using only the adsorption reaction in Eq. (12), a very weak displacement of the IEP to slightly higher pH values of about 5.5 results depending on the specific conditions. However, the reaction in Eq. (14) causes a much stronger displacement of the IEP to lower pH values, again depending on the specific conditions.

Although measurement of the IEP was not carried out in the present study, strong decreases in the IEP have been reported for the aspartate–anatase system (Giacomelli et al., 1995) and the glutamate–rutile system (Fuerstenau et al., 1984). For the aspartate–anatase system in 0.03 M KNO_3 , a decrease of the IEP from 6.0 without aspartate to 5.2 in the presence of 1.0 mM aspartate was reported, i.e. a decrease of 0.8 pH units. Unfortunately, the solid concentration was not reported, so a detailed comparison with this result is not possible. However, the direction of the decrease in the IEP is important because it provides a qualitative test of the surface complexation reactions adopted in the present study.

Using our surface complexation model for the aspartate–rutile system in 0.03 M NaCl solutions, we predicted a decrease in the IEP from 5.4 without aspartate to 4.8 in the presence of 1.0 mM aspartate at a solid concentration of 20 g L^{-1} , i.e. a decrease of 0.6 pH units. The surface speciation of aspartate under these conditions is similar to that in Fig. 5c, i.e. both surface species are present in similar abundances. At lower solid concentrations, for example, 2.0 g L^{-1} , taking into account the effect of solid concentration on the equilibrium constant for Eq. (14) referring to the hypothetical 1.0 M standard state, the predicted decrease of the IEP is 0.7 pH units. The predicted decreases are relatively insensitive to the solid concentration in the model for this system because the main part of the decrease is associated with the reaction in Eq. (14) rather than Eq. (12). The equilibrium constant for Eq. (14) does not depend on solid concentration when referred to the hypothetical 1.0 M standard state. Consequently, the model predictions made here of decreases of 0.6–0.7 in the IEP are consistent with both the direction and magnitude of the shift of 0.8 reported for aspartate by Giacomelli et al. (1995). This result provides additional evidence of the validity of the reaction stoichiometries established in the present study.

3.4. Prediction of aspartate surface speciation

The predicted surface speciation of aspartate as a function of pH, ligand-to-solid ratio and ionic strength is shown in Fig. 5a–d. It can be seen in these figures that the predicted proportions of the two surface aspartate species vary strongly with environmental conditions. The bridging-bidentate species is at its maximum importance at the lowest pH values, and is always the most abundant species up to pH values of about 5. It is most strongly predominant at the lower aspartate concentrations and the highest ionic strength (Fig. 5a and d). Under most other conditions, the predominant surface species of aspartate is the outer-sphere species. With increases in ionic strength, the bridging-bidentate adsorption is barely affected, whereas the

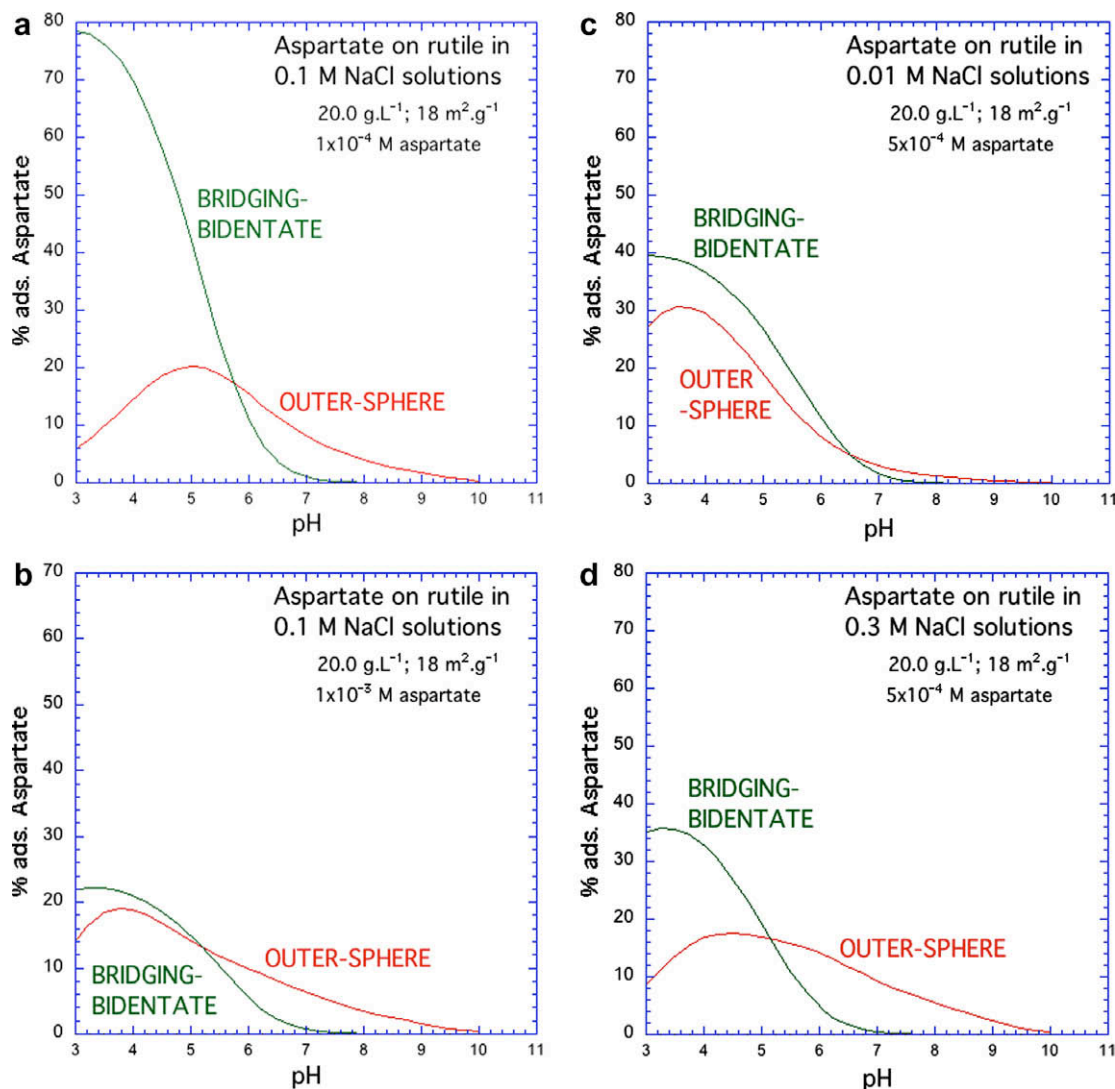


Fig. 5. Predicted surface speciation of aspartate on rutile as a function of ligand concentration and ionic strength. The species names bridging-bidentate and outer-sphere refer to the pictures in Fig. 3a and c, and the reaction stoichiometries in Eqs. (12) and (14), respectively.

outer-sphere species adsorption is diminished and broadened with respect to pH (Fig. 5c and d). It can be seen that the outer-sphere species is predicted to have a maximum concentration at pH values of about 4–6, depending on the ionic strength and the total aspartate concentration.

4. CONCLUDING REMARKS

Batch adsorption experiments and potentiometric titration measurements at 25 °C and 1 bar over a broad range of pH, ligand-to-solid ratio and ionic strength were used to elucidate the possible modes of adsorption of L-aspartate on the surface of rutile (α -TiO₂). Results show that the adsorption of aspartate on rutile is favored at pH below 6. The decrease in adsorption at higher pH reflects the unfavorable electrostatic conditions for a negatively charged aspartate molecule to adsorb to a negatively charged surface. At pH values of 3–5, aspartate adsorption increases with decreasing ionic strength.

The extended triple-layer model was used to develop a quantitative thermodynamic characterization of aspartate adsorption. Two reaction stoichiometries were needed to describe the experimental data. One involved a possible bridging-bidentate surface species binding through both carboxyl groups, which can be thought of as “lying down” on the surface consistent with previous ATR-FTIR interpretations of aspartate adsorption on amorphous TiO₂ and our results for glutamate on the same rutile. The other reaction stoichiometry involved a likely outer-sphere or hydrogen bonded aspartate surface species, possibly “standing up” at the rutile surface.

The surface complexation model was tested against experimental data for the potentiometric titration of aspartate in the presence of rutile. In addition, the model correctly predicted a strong decrease of the isoelectric point with increased aspartate concentration consistent with previously published studies of the aspartate-anatase system (Giacomelli et al., 1995). Both of these comparisons provide strong support

for the applicability of the reaction stoichiometries for aspartate adsorption in the surface complexation model. The use of complementary techniques thus provides an extended understanding of aspartate–rutile interactions.

In comparison with our previous work with glutamate on rutile (Jonsson et al., 2009), it is interesting to note that aspartate and glutamate show similar adsorption behavior, although a slightly higher amount of adsorbed aspartate is observed per m² of rutile at pH values of 3–5. Also, the adsorption trends of both amino acids show similar ionic strength dependence. We emphasize that these features can be accounted for by the same reaction stoichiometries. However, these stoichiometries can be interpreted in different ways. We interpret the mode of attachment of aspartate and glutamate at low surface coverages to be the same, i.e. the bridging-bidentate species involving two inner-sphere and two hydrogen bonded linkages to the surface. However, based on the published infrared spectroscopic results discussed above, we interpret the mode of attachment of aspartate and glutamate at high surface coverages to be different. For aspartate we infer an outer-sphere or hydrogen bonded species and for glutamate a species involving one inner-sphere and one hydrogen bonded linkage to the surface. For both aspartate and glutamate, the predicted proportions of the two complexes on the surface of rutile are a strong function of the environmental conditions, which should be taken into account in considerations of geochemical systems involving the interactions of biomolecules and mineral surfaces. This result is of fundamental interest and may have implications for a wide range of geochemical processes from biomineralization to the role of mineral surface in the origin of life.

ACKNOWLEDGMENTS

The authors are grateful for the specially cleaned rutile powder sample provided to them by J. Rosenqvist and D. Wesolowski (Oak Ridge National Laboratory) and M. Machesky (Illinois State Water Survey). We appreciate discussions with G.D. Cody, J.A. Davis, P. Fenter, M. Fogel, A.J. McQuillan, J. Rosenqvist and D.L. Sparks. N. Lee helped in the laboratory and in discussions of the results. Financial support was provided by a joint National Science Foundation—NASA Astrobiology Institute Collaborative Research Grant to the Johns Hopkins University and the Carnegie Institution for Science. D.A. Sverjensky, C.M. Jonsson, C.L. Jonsson and C. Estrada express their appreciation for the facilities and hospitality extended to them by the Geophysical Laboratory of the Carnegie Institution of Washington. C. Estrada wishes to acknowledge support from the National Science Foundation—Research Experience for Undergraduates Program administered at the Geophysical Laboratory by S. Gramsch. In addition, the authors would like to thank M. Machesky and three anonymous reviewers for comments that resulted in significant improvements of this manuscript.

APPENDIX A. SUPPLEMENTARY DATA

Supplementary data associated with this article can be found, in the online version, at [doi:10.1016/j.gca.2010.01.003](https://doi.org/10.1016/j.gca.2010.01.003).

REFERENCES

- Brunauer S., Emmett P. H. and Teller E. (1938) Adsorption of gases in multimolecular layers. *J. Am. Chem. Soc.* **60**, 309–319.
- Catalano J. G., Zhang Z., Fenter P. and Bedzyk M. J. (2006) Inner-sphere adsorption geometry of Se(IV) at the hematite (1 0 0)–water interface. *J. Colloid Interface Sci.* **297**, 665–671.
- Catalano J. G., Zhang Z., Park C. Y., Fenter P. and Bedzyk M. J. (2007) Bridging arsenate surface complexes on the hematite (0 1 2) surface. *Geochim. Cosmochim. Acta* **71**, 1883–1897.
- Costa D., Tougerti A., Tielens F., Gervais C., Stievano L. and Lambert J. F. (2008) DFT study of the adsorption of microsolvated glycine on a hydrophilic amorphous silica surface. *Phys. Chem. Chem. Phys.* **10**, 6360–6368.
- Criscenti L. J. and Sverjensky D. A. (2002) A single-site model for divalent transition and heavy metal adsorption over a range of metal concentrations. *J. Colloid Interface Sci.* **253**, 329–352.
- De Robertis A., De Stefano C. and Gianguzza A. (1991) Salt effects on the protonation of L-histidine and L-aspartic acid—a complex-formation model. *Thermochim. Acta* **177**, 39–57.
- De Yoreo J. J., Wierzbicki A. and Dove P. M. (2007) New insights into mechanisms of biomolecular control on growth of inorganic crystals. *Cryst. Eng. Comm.* **9**, 1144–1152.
- Elhadj S., De Yoreo J. J., Hoyer J. R. and Dove P. M. (2006a) Role of molecular charge and hydrophilicity in regulating the kinetics of crystal growth. *Proc. Natl. Acad. Sci. USA* **103**, 19237–19242.
- Elhadj S., Salter E. A., Wierzbicki A., De Yoreo J. J., Han N. and Dove P. M. (2006b) Peptide controls on calcite mineralization: Polyaspartate chain length affects growth kinetics and acts as a stereochemical switch on morphology. *Cryst. Growth Des.* **6**, 197–201.
- Fedkin M. V., Zhou X. Y. Y., Kubicki J. D., Bandura A. V., Lvov S. N., Machesky M. L. and Wesolowski D. J. (2003) High temperature microelectrophoresis studies of the rutile/aqueous solution interface. *Langmuir* **19**, 3797–3804.
- Fuerstenau D. W., Chander S., Lin J. and Parfitt G. D. (1984) Adsorption and electrokinetic effects of amino acids on rutile and hydroxyapatite. *ACS Symp. Ser.* **253**, 311–327.
- Fukushi K. and Sverjensky D. A. (2007) A predictive model (ETLM) for arsenate adsorption and surface speciation on oxides consistent with spectroscopic and theoretical molecular evidence. *Geochim. Cosmochim. Acta* **71**, 3717–3745.
- Giacomelli C. E., Avena M. J. and Depauli C. P. (1995) Aspartic acid adsorption onto TiO₂ particles surface—experimental data and model calculations. *Langmuir* **11**, 3483–3490.
- Goldschmidt V. M. (1952) Geochemical aspects of the origin of complex organic molecules on the Earth, as precursors to organic life. *New Biol.* **12**, 97–105.
- Hazen R. M. (2006) Mineral surfaces and the prebiotic selection and organization of biomolecules. *Am. Mineral.* **91**, 1715–1729.
- Hazen R. M., Papineau D., Leeker W. B., Downs R. T., Ferry J. M., McCoy T. J., Sverjensky D. A. and Yang H. X. (2008) Mineral evolution. *Am. Mineral.* **93**, 1693–1720.
- Helgeson H. C., Kirkham D. H. and Flowers G. C. (1981) Theoretical prediction of the thermodynamic behavior of aqueous electrolytes at high pressures and temperatures. IV. Calculation of activity coefficients, osmotic coefficients, and apparent molal and standard and relative partial molal properties to 600 °C and 5 Kb. *Am. J. Sci.* **281**, 1249–1516.
- Ikhsan J., Johnson B. B., Wells J. D. and Angove M. J. (2004a) Adsorption of aspartic acid on kaolinite. *J. Colloid Interface Sci.* **273**, 1–5.
- Ikhsan J., Wells J. D., Johnson B. B. and Angove M. J. (2004b) The effect of aspartic acid on the binding of transition metals to kaolinite. *J. Colloid Interface Sci.* **273**, 6–13.

- Jonsson C. M., Jonsson C. L., Sverjensky D. A., Cleaves H. J. and Hazen R. M. (2009) Attachment of L-glutamate to rutile (α -TiO₂): a potentiometric, adsorption and surface complexation study. *Langmuir* **25**, 12127–12135.
- Lambert J. F. (2008) Adsorption and polymerization of amino acids on mineral surfaces: a review. *Orig. Life Evol. Biosph.* **38**, 211–242.
- Lambert J. F., Stievano L., Lopes I., Gharsallah M. and Piao L. Y. (2009) The fate of amino acids adsorbed on mineral matter. *Planet. Space Sci.* **57**, 460–467.
- Machesky M. L., Wesolowski D. J., Palmer D. A. and Ichiro-Hayashi K. (1998) Potentiometric titrations of rutile suspensions to 250 °C. *J. Colloid Interface Sci.* **200**, 298–309.
- Ridley M. K., Machesky M. L., Palmer D. A. and Wesolowski D. J. (2002) Potentiometric studies of the rutile-water interface. Hydrogen-electrode concentration-cell versus glass-electrode titrations. *Colloid Surf. A—Physicochem. Eng. Asp.* **204**, 295–308.
- Ridley M. K., Machesky M. L., Wesolowski D. J. and Palmer D. A. (1999) Calcium adsorption at the rutile-water interface: a potentiometric study in NaCl media to 250 °C. *Geochim. Cosmochim. Acta* **63**, 3087–3096.
- Ridley M. K., Machesky M. L., Wesolowski D. J. and Palmer D. A. (2004) Modeling the surface complexation of calcium at the rutile-water interface to 250 °C. *Geochim. Cosmochim. Acta* **68**, 239–251.
- Ridley M. K., Machesky M. L., Wesolowski D. J. and Palmer D. A. (2005) Surface complexation of neodymium at the rutile-water interface: a potentiometric and modeling study in NaCl media to 250 °C. *Geochim. Cosmochim. Acta* **69**, 63–81.
- Roddick-Lanzilotta A. D. and McQuillan A. J. (2000) An in situ infrared spectroscopic study of glutamic acid and of aspartic acid adsorbed on TiO₂: implications for the biocompatibility of titanium. *J. Colloid Interface Sci.* **227**, 48–54.
- Sahai N. and Sverjensky D. A. (1998) GEOSURF: a computer program for modeling adsorption on mineral surfaces from aqueous solution. *Comput. Geosci.* **24**, 853–873.
- Stephenson A. E., DeYoreo J. J., Wu L., Wu K. J., Hoyer J. and Dove P. M. (2008) Peptides enhance magnesium signature in calcite: insights into origins of vital effects. *Science* **322**, 724–727.
- Sverjensky D. A. (2003) Standard states for the activities of mineral surface sites and species. *Geochim. Cosmochim. Acta* **67**, 17–28.
- Sverjensky D. A. (2005) Prediction of surface charge on oxides in salt solutions: revisions for 1:1 (M⁺L⁻) electrolytes. *Geochim. Cosmochim. Acta* **69**, 225–257.
- Sverjensky D. A. (2006) Prediction of the speciation of alkaline earths adsorbed on mineral surfaces in salt solutions. *Geochim. Cosmochim. Acta* **70**, 2427–2453.
- Sverjensky D. A. and Fukushi K. (2006a) A predictive model (ETLM) for As(III) adsorption and surface speciation on oxides consistent with spectroscopic data. *Geochim. Cosmochim. Acta* **70**, 3778–3802.
- Sverjensky D. A. and Fukushi K. (2006b) Anion adsorption on oxide surfaces: inclusion of the water dipole in modeling the electrostatics of ligand exchange. *Environ. Sci. Technol.* **40**, 263–271.
- Sverjensky D. A., Jonsson C. M., Jonsson C. L., Cleaves H. J. and Hazen R. M. (2008) Glutamate surface speciation on amorphous titanium dioxide and hydrous ferric oxide. *Environ. Sci. Technol.* **42**, 6034–6039.
- Teng H. H. and Dove P. M. (1997) Surface site-specific interactions of aspartate with calcite during dissolution: implications for biomineralization. *Am. Mineral.* **82**, 878–887.
- Tsirtos A. and Nancollas G. H. (1999) The adsorption of polyelectrolytes on hydroxyapatite crystals. *J. Colloid Interface Sci.* **209**, 109–115.
- Tsirtos A. and Nancollas G. H. (2002) The role of polycarboxylic acids in calcium phosphate mineralization. *J. Colloid Interface Sci.* **250**, 159–167.
- Zhang Z., Fenter P., Cheng L., Sturchio N. C., Bedzyk M. J., Predota M., Bandura A., Kubicki J. D., Lvov S. N., Cummings P. T., Chialvo A. A., Ridley M. K., Benezeth P., Anovitz L., Palmer D. A., Machesky M. L. and Wesolowski D. J. (2004) Ion adsorption at the rutile-water interface: linking molecular and macroscopic properties. *Langmuir* **20**, 4954–4969.

Associate editor: Michael L. Machesky